Laser micro-Raman spectroscopy of single-point diamond machined silicon substrates

Jiwang Yan[a)]
Department of Mechanical Engineering, Kitami Institute of Technology, Koen-cho 165, Kitami, Hokkaido 090-8507, Japan

(Received 11 September 2003; accepted 17 November 2003)

Laser micro-Raman spectroscopy was used to examine the silicon substrates machined by single-point diamond turning at machining scales ranging from 10 to 1000 nm under plane strain conditions. The results showed that the subsurface layer was partially transformed to amorphous, the extent of amorphization depending strongly on the undeformed chip thickness. The intensities of the crystalline phase and the amorphous phase show opposite tendencies with respect to the undeformed chip thickness. In brittle regime machining, Raman spectra differ depending on the test locations. The intensity of the amorphous phase reaches maximum near the ductile–brittle transition boundary. In ductile regime machining, the intensity of the amorphous phase decreased sharply as the undeformed chip thickness decreased. This work provides technological insights into the possibility of direct manufacturing of subsurface damage-free optical and optoelectronic products of silicon by ductile machining without the need for or with a decreased need for subsequent etching or chemomechanical polishing. © *2004 American Institute of Physics.* [DOI: 10.1063/1.1639953]

I. INTRODUCTION

Single-crystal silicon is not only a dominant substrate material for the fabrication of microelectronic and micromechanical components but also an important infrared optical material.[1,2] Due to its hard and brittle nature, silicon is currently finished by lapping and chemomechanical polishing (CMP). However, silicon can be plastically deformed in a ductile manner in ultraprecision machining at an extremely small machining scale down to the range of a submicrometer, yielding continuous ductile chips and extremely smooth surfaces.[3–6] The ductile machining technology requires the use of an extremely rigid, environmentally controlled, ultraprecision machine tool and a single-crystal diamond tool with a negative rake angle.[7] Using the ductile machining technology, the productivity of aspherical, diffractive optical components, and large-diameter substrates for recent microelectronic mechanical system (MEMS) applications can be significantly improved.

However, currently, ductile machining technology has not yet been widely used as the final finishing process for silicon substrates; instead, it is usually followed by subsequent processing. The most important factor restricting the use of ductile machining technology is the subsurface damage generated during machining, which involves microstructure change, dislocations, and microcracks. It is the depth and nature of the subsurface damage that influences the mechanical, optical, and electronic performances of silicon products. For example, in high-power laser optics, the lifetime of optical components depends strongly on the near-surface structures of the crystals. For most optoelectronic and MEMS applications, additional etching and/or CMP processes are required to remove the subsurface damaged layer. Thus, eliminating the subsurface damage during diamond machining will bring about immense cost reductions and solve the environmental problems caused by the CMP and etching processes. Fabricating subsurface-damage-free silicon substrates is also essential for producing high-reliability ultraprecision optical, mechanical, and electronic parts. Recently, the direct production of subsurface-damage-free silicon components by ductile machining technology has become a subject of concentrated research interests from the viewpoints of the microelectronics, optoelectronics, and manufacturing industries.

Previous studies revealed that semiconductors, such as silicon and germanium, undergo structural changes during machining and scratching.[8–10] Tanikella *et al.*[11] confirmed the presence of an amorphous phase within microcutting grooves scratched on single-crystal silicon surfaces and in the cutting debris outside of the grooves. Cross-sectional transmission electron microscopy (TEM) studies of a diamond turned silicon surface conducted by Shibata *et al.*[12] revealed that a 150-nm-thick amorphous layer was formed, below which is a region of crystal about 2–3 μm deep deformed by shear dislocation loops. The TEM results of Jeynes *et al.*[13] showed that a 110-nm-thick amorphous layer, below which a region of crystal about 260 nm deep with dislocation, was formed during diamond turning. Puttick *et al.*[8] demonstrated that the mean depth of the subsurface damage layer of both diamond turned and ground silicon is in the range of 100–400 nm, and that amorphous phase existed in the near-surface layer in both cases. Puttick *et al.*[8] also pointed out that the subsurface damage due to grinding was highly variable and irregular compared to that of diamond turning. Recently, the work of Gogotsi *et al.*[14] demonstrated that phase transformations also occur in other silicon machining processes including slicing and dicing. However, to date, the physics governing the subsurface damaging

a)Electronic mail: yanjw@mail.kitami-it.ac.jp

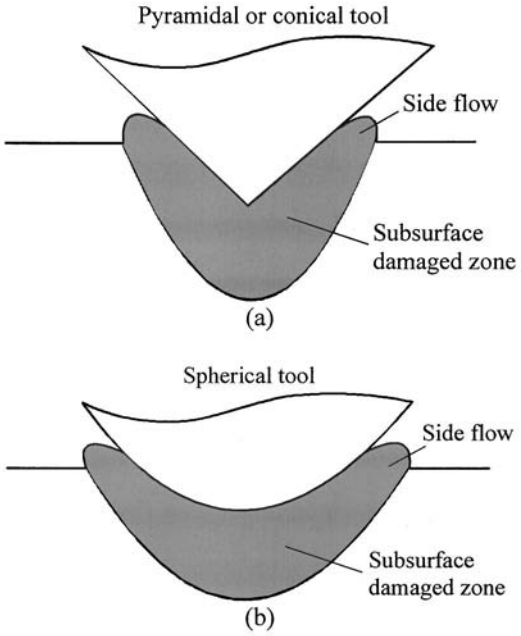

FIG. 1. Schematics of the subsurface damage zones produced by (a) conical or pyramidal tools and (b) spherical tools. On both occasions, due to the nonorthogonal cutting conditions, side flows take place and the resulting subsurface structure is location dependent.

mechanism has not been well understood, and the relationships between the subsurface damage and the machining conditions remain to be investigated.

As a complete understanding of the subsurface damage of the diamond machined silicon can only follow an understanding of the individual mechanisms, the work reported here is focused exclusively on the relationship between the machining conditions and the subsurface phase transformation, namely, amorphization. In order to accomplish direct, quick, and nondestructive measurement of the subsurface amorphization of silicon, we used laser micro-Raman spectroscopy. Laser micro-Raman spectroscopy is known as a powerful characterization technique for various semiconductor and insulator materials at a spatial resolution down to the excitation wavelength. The Raman effect is based on an inelastic light-scattering process and occurs when a beam of monochromatic light passes through a crystal. The vibration spectrum of the material is strongly influenced by microscopic structural changes (long- and short-range disorders), impurity, and residual strains, which lead to changes in phonon frequencies, broadening of Raman peaks, and breakdown of Raman selection rules. Thus, the method can detect the presence of amorphous silicon (a-Si) as well as residual stresses that may be present. Recently, laser micro-Raman spectroscopy has been used to map the structural change and residual stress of silicon in scratching, dicing, lapping, and grinding processes.[14–16]

In most available literature involving laser micro-Raman spectroscopic studies of machined silicon surfaces, spherical, conical, or pyramidal diamond tips or indenters[11,15] were used to produce individual scratching grooves, as schematically shown in Figs. 1(a) and 1(b), to simulate the abrasive machining processes. However, these tool geometries lead to

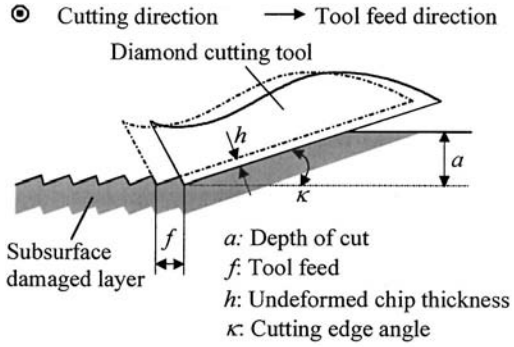

FIG. 2. Schematic of the subsurface damage layer produced by single-point diamond turning with a straight-nosed cutting tool. Under the plain strain cutting conditions, the resulting subsurface structure is uniform and location independent.

nonorthogonal cutting, where the machining scale, namely, the undeformed chip thickness, varies from point to point along the tool contours even at the same section of a cutting groove. Also, significant side flow of the work materials takes place.[11,15] Hence, the resulting subsurface structures beneath the tool will not be uniform but dependent on the location. Because the width of the microgroove is on the same level as the laser spot size of the laser micro-Raman tests, sometimes the location dependence of the subsurface structure makes it difficult to accurately characterize the relationship between the machining scale and the subsurface damage. In addition, the scratching speeds used in the previous works were extremely low (0.005–0.01 m/s)[11,15] compared to that of the practical diamond machining processes.

In the present work, we conducted single-point diamond turning on silicon substrates at a speed level of a few m/s, approximately one hundred times higher than the scratching speed. A single-point diamond cutting tool with an extremely sharp straight cutting edge, namely, a straight-nosed diamond tool, is adopted in order to produce uniform continuous surfaces for laser micro-Raman tests. Thus, the undeformed chip thickness will be consistent over the entire cutting width and hence provide the plain strain conditions, that is, the orthogonal cutting conditions, without side flow. The machining scale can be precisely controlled from the micrometer level down to the nanometric level through the numerical control of the ultraprecision machine. Thus, this method enables the direct and unambiguous correspondence between the machining scale and the laser micro-Raman spectroscopy. The objective of this work is to explore quantitatively the relationships between the subsurface amorphization and the machining conditions and assist in finding possible solutions to minimize the subsurface damages.

II. EXPERIMENTAL PROCEDURES

A. Diamond tool

The machining model of a straight-nosed cutting tool[17] is schematically shown in Fig. 2. In this case, the tool is subjected to a transverse feed (f) per revolution of the workpiece; hence, a large-area surface consisting of extremely fine parallel grooves can be produced. Because the unde-

formed chip thickness (h) is uniform across the entire width of the cutting edge, the entire machined surface will have a uniform subsurface microstructure. Thus, the relationships between surface/subsurface structure and undeformed chip thickness are unambiguous and can be readily compared. The relationship between undeformed chip thickness h, cutting edge angle κ, and tool feed f can be described by

$$h = f \times \sin \kappa. \tag{1}$$

Thus, by using a sufficiently small κ and/or a sufficiently small f, it is possible to thin the undeformed chip thickness h to the nanometric range over the entire cutting region.

The theoretical surface roughness generated by a straight-nosed tool is determined by the tool feed f and the cutting edge angle κ. Usually, this surface roughness is higher than that generated by a conventional round-nosed tool.[3–5] However, by using an extremely small cutting edge angle ($\sim 0.1°$),[17] it is possible for the straight-nosed tool to achieve very low surface roughness which is comparable to that generated by a round-nosed tool. The combination of a high tool feed and an extremely small cutting edge angle enables high-efficiency ductile machining.[17]

In the present experiments, a single-crystal diamond cutting tool that has a 1.2-mm-straight edge, a $-30°$ rake angle, and a 6° relief angle was used. The $-30°$ rake angle is used to achieve both high ductile machinability and relatively low cutting forces.[18] The tool edge was examined by an atomic force microscope and the edge radius (roundness) was estimated to be ~ 50 nm. Cutting silicon with diamond tools produces aggressive tool wear, which can change the ductile–brittle response. It is empirically known that the tool wear begins to affect the ductile–brittle transition from a cutting distance of approximately 5 km.[19] In this study, in order to keep the tool wear within a negligible range, the experiments were designed to make the cumulative cutting distance of all the cutting tests shorter than 0.6 km.

B. Ultraprecision machining apparatus

The experiments were carried out on a three-axis numerically controlled ultraprecision diamond lathe, NACHI-ASP15 produced by Nachi-Fujikoshi Corp., Japan. The machine has an ultraprecision air-bearing spindle, two perpendicular linear tables, and a rotary table. The linear tables are supported by high-stiffness hydrostatic bearings and are driven by servomotors via hydrostatic screws, allowing smooth nanometric movement with negligible mechanical friction. The rotary table is also supported by hydrostatic bearings and driven by a friction drive in order to protect it from nondriven backlash movements. Laser hologram scales are used to accurately position all of these tables. Under precise numerical control, the linear tables can be moved by 10 nm per step and the rotary table can be rotated with an angular resolution of 0.001°. To isolate the machine from environmental vibration, the main section of the machine was fixed to a granite bed, which is supported by a set of air mounts.

C. Specimens

Device grade p-type single-crystal silicon wafers having a doping level of 1.33×10^{14} atoms/cm^3, produced by Sumitomo Mitsubishi Silicon Corporation, Japan were used as specimens. The surface orientation of these silicon wafers is (111). These wafers are 76.2 mm in diameter, 1.2 mm in thickness, and obtained with chemomechanical polished finishes. To avoid cutting the workpiece center where the cutting speed approaches zero, the center area of the wafer within a diameter of 20 mm was removed before the experiment. The workpieces were bonded on diamond-turned aluminum blanks using a heat-softened glue and then vacuum-chucked to the machine spindle.

D. Machining conditions

Undeformed chip thickness h was varied from 10 to 1000 nm by changing the tool feed f in the ranges of 0.5–50 μm with the cutting edge angle κ fixed to 1.146°. The depth of cut (a) was set to 2 μm. The rotation rate of the machine spindle was fixed to 1500 rpm, and consequently, the cutting speed changes from 1.57 to 5.98 m/s during facing cuts. This cutting speed is far higher than the speed used in the scratching tests.[11,15] Dry cutting is performed without any cutting fluid to avoid any contamination or chemical effects.

E. Surface characterization method

The machined silicon substrates were first observed with a Nomarski differential interferential microscope to examine them for the presence of surface damage, and then measured using a laser-scanning three-dimensional measurement system, VK-8550, (Keyence Corp., Japan) in order to obtain three-dimensional surface topographies. Subsequently, a laser micro-Raman spectroscope, NRS-2100 (JASCO Corp., Japan), was used to characterize the subsurface damage. The wavelength of the laser in the micro-Raman test was 514.5 nm and the output laser power was 4 mV. Under these conditions, the penetration depth of the laser into pristine silicon was approximately 1 μm.[16,20] For amorphous silicon, the optical absorption coefficient is higher, leading to a smaller penetration depth. The 100 times objective lens was used so that the focused laser spot size was 1 μm. This spot size is sufficiently small compared with the sizes of microfractures on the objective surface, enabling the precise location of test points when measuring the brittle regime machined surfaces. This way, the averaging effect which occurs in conventional laser macro-Raman tests[21] can be avoided. In order to diminish experimental errors, all of the measurements were performed under the same strictly controlled conditions at room temperature. Moreover, in order to avoid the influences of the substrate crystal orientation, in this study, all of the measurements were performed at the same substrate orientation where the cutting direction was in the $[11\bar{2}]$ direction. This is the orientation most difficult to be ductile machined.[17] Changing the cutting direction will cause changes in machining response. The effect of crystal orientation on subsurface damage will be further investigated and discussed elsewhere.

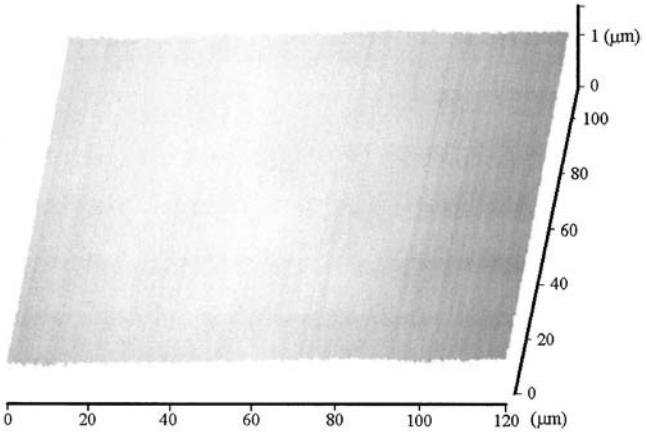

FIG. 3. Scanning laser microscopic topography of the machined silicon surface at an undeformed chip thickness of 20 nm, indicating a completely ductile machining regime.

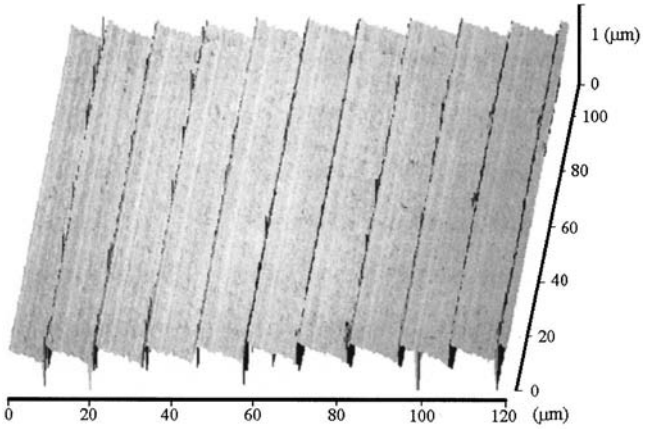

FIG. 4. Scanning laser microscopic topography of the machined silicon surface at an undeformed chip thickness of 200 nm, indicating a ductile–brittle transition machining regime.

III. RESULTS

A. Surface topography

First, the critical undeformed chip thickness (alternatively termed the critical depth of cut, d_c) for the ductile–brittle transition was measured. This is done by performing a facing cut on a small region of a workpiece at continuously varied tool feeds (0.5–50 μm) at a constant cutting edge angle (1.146°), as described in a previous paper.[17] This gives rises to a continuous change of the undeformed chip thickness from 10 to 1000 nm. The machined surface was then observed with a Nomarski microscope, and the ductile–brittle transition boundary where microfractures begin to take place can be identified. The value of d_c was obtained by measuring the critical tool feed (f_c) at the brittle–ductile transition boundary. In the present experiment, f_c was 7.5 μm, thus, the critical undeformed chip thickness d_c was 150 nm according to Eq. (1). Next, undeformed chip thickness h was set to ten levels: 10, 20, 50, 100, 200, 300, 400, 600, 800, and 1000 nm, by changing the tool feed step by step, and the machined surfaces were characterized.

Figures 3–5 show the three-dimensional topographies of the surfaces machined at undeformed chip thicknesses of 20, 200, and 800 nm, respectively. At an undeformed chip thickness of 20 nm, as shown in Fig. 3, the machined surface is extremely smooth, showing no evidence of damage across the entire surface. The surface roughness was on the level of a few nanometers. This kind of surface topography indicates that the surface has been produced through a completely ductile regime material removal. Figure 4 shows the surface machined at an undeformed chip thickness of 200 nm. The surface consists of regular microgrooves formed by periodical cross tool feeds. Besides the saw-toothed tool feed profiles, a few extremely small microcracks, approximately 1 μm in size, can be observed. This kind of surface topography indicates that the machining mode has gone beyond the crack-initiation threshold and transitioned to the brittle regime. When the undeformed chip thickness is further increased to 800 nm, as shown in Fig. 5, the resulting surface is far from smooth, and is pitted with microfractures, the sizes of which range on the order of 1–10 μm. This kind of surface indicates that brittle fracture has been predominant in the material removal process.

B. Raman spectra

It is known from previous literature that for bulk crystalline silicon (c-Si), the triple degenerate optical phonons display in the first-order Raman spectrum a sharp peak at the Raman shift of 521 cm^{-1}, and for a-Si, the first-order Raman spectrum reflects the phonon density of states and presents an optical band peak at 470 cm^{-1}.[21–23] In this study, Raman spectra in the Raman shift range of 200–600 cm^{-1} were measured, which covers the range of the characteristic peaks associated with c-Si and a-Si.

Figure 6 shows the laser micro-Raman spectrum of the surface machined at an undeformed chip thickness of 20 nm, as shown in Fig. 3. There is a characteristic Raman peak of c-Si at 521 cm^{-1}, whereas the intensity at other frequencies is negligibly low. This indicates that the subsurface layer is mainly crystalline.

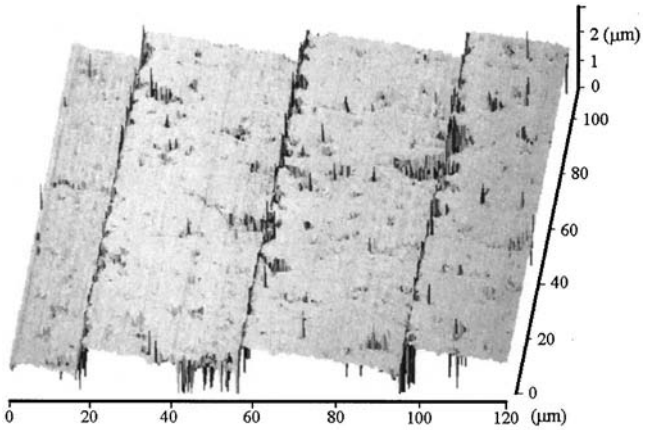

FIG. 5. Scanning laser microscopic topography of the machined silicon surface at an undeformed chip thickness of 800 nm, showing a brittle machining regime involving numerous microfractures.

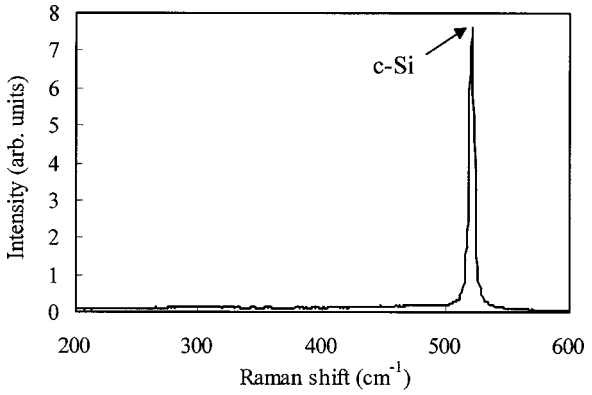

FIG. 6. Laser micro-Raman spectrum at an undeformed chip thickness of 20 nm. There is a characteristic Raman peak of crystalline Si at 521 cm^{-1}, indicating that the subsurface layer is mainly crystalline.

As the undeformed chip thickness increased to 50 nm, as shown in Fig. 7, the intensity of the Raman peak of *c*-Si at 521 cm^{-1} clearly became lower than that in Fig. 6. However, a significant broadband peak centered at 470 cm^{-1} appears, indicating that the subsurface layer has been partially transformed into an amorphous state.

Figure 8 shows the Raman spectrum of the surface machined at an undeformed chip thickness of 200 nm, as shown in Fig. 4. The broadband peak at 470 cm^{-1} becomes more significant, whereas no peak can be observed at 521 cm^{-1}. The lack of feature at 521 cm^{-1} is indicative of the absence of *c*-Si and indicates that the subsurface layer within the laser penetration depth has been completely transformed into an amorphous state.

As the undeformed chip thickness was further increased to be more than 300 nm, the measurement results of Raman spectra began to differ distinctly depending on the location of the test points, that is, in the nonfractured or fractured area. Figure 9(a) shows the Raman spectrum of the nonfractured areas of the surface machined at an undeformed chip thickness of 800 nm, as shown in Fig. 5. In Fig. 9(a), both a small peak at 521 cm^{-1} and a broadband peak at 470 cm^{-1} can be observed. However, as shown in Fig. 9(b), when the laser spot was located within the microfractures, only the

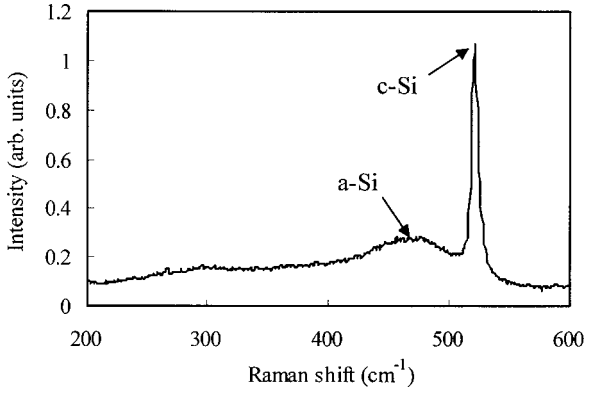

FIG. 7. Laser micro-Raman spectrum at an undeformed chip thickness of 50 nm. A significant broadband peak centered at 470 cm^{-1} appears apart from the *c*-Si peak, indicating that the subsurface layer has been partially transformed into the amorphous state.

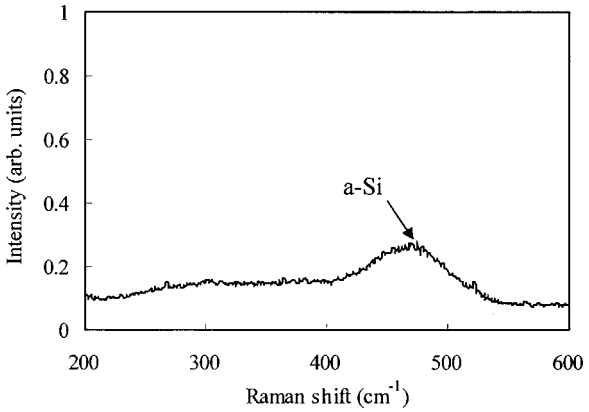

FIG. 8. Laser micro-Raman spectrum at an undeformed chip thickness of 200 nm. The broadband peak centered at 470 cm^{-1} is predominant, indicating that the subsurface layer within the measurement range has been almost completely transformed into the amorphous state.

peaks at 521 cm^{-1} appeared while no peak appeared at 470 cm^{-1}, which indicates the absence of the amorphous phase.

C. Raman intensity

Next, the Raman intensities (arbitrary unit) of the crystalline and amorphous phases were compared and plotted with respect to the undeformed chip thickness. For the brittle

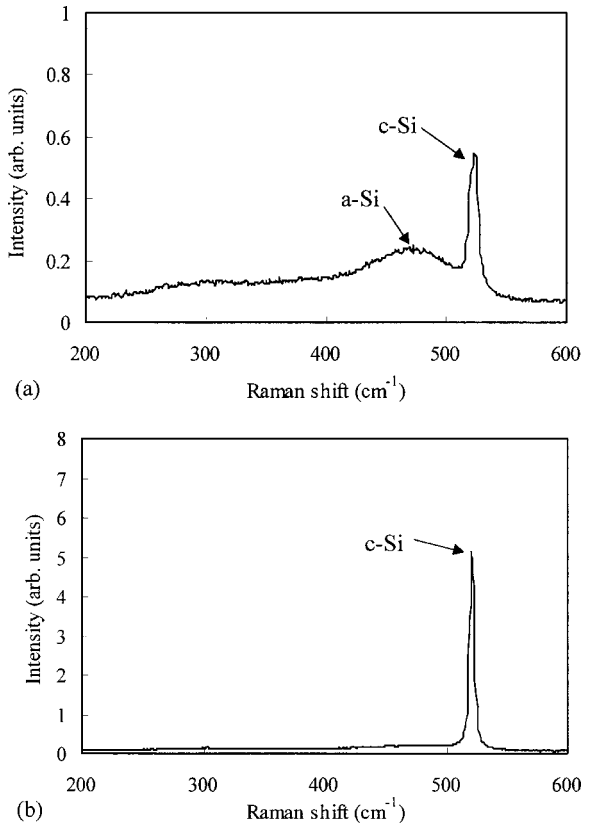

FIG. 9. Laser micro-Raman spectra at an undeformed chip thickness of 800 nm. The measurement results of Raman spectra differ distinctly depending on the location of the test points: (a) nonfractured area, and (b) fractured area.

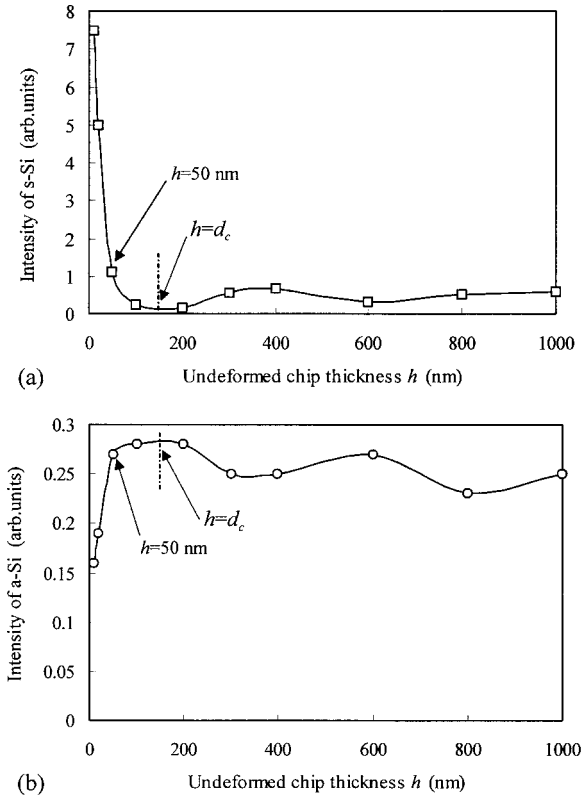

FIG. 10. Plots of the Raman intensities of (a) crystalline phase and (b) amorphous phase with respect to undeformed chip thickness. The two curves change oppositely with respect to undeformed chip thickness. The intensity of crystalline phase becomes maximum and the intensity of the amorphous phase becomes minimum near the ductile–brittle transition boundary.

regime machined surfaces pitted with microfractures, the Raman intensities of the nonfractured areas were plotted. Figure 10(a) shows the variation of Raman intensities of the crystalline phase (c-Si) at 521 cm^{-1} as the undeformed chip thickness changes. The intensity of c-Si drops rapidly as the undeformed chip thickness increases from 10 nm to 50 nm, reaches a minimum between 100–200 nm, and tends to be constant when the undeformed chip thicknessis more than 300 nm. Figure 10(b) shows the variation of the Raman intensity of the amorphous phase (a-Si) at 470 cm^{-1} with the undeformed chip thickness. The intensity of a-Si increases sharply as the undeformed chip thickness increases from 10 nm to 50 nm, reaches a maximum between 100–200 nm, and tends to be constant as the undeformed chip thickness is further increased from 300 nm. Based on these results, it is evident that the Raman intensities of the crystalline phase and amorphous phase change oppositely with respect to the undeformed chip thickness. It is also worth noting that the maximum intensity of the crystalline phase and the minimum intensity of the amorphous phase both take place near the ductile–brittle transition boundary, that is, the undeformed chip thickness of 150 nm.

IV. DISCUSSION

While the issue of the origin of amorphization during silicon machining is a controversial one and is still under investigation, a possible reason may be the high hydrostatic pressures resulting from the tool–workpiece contact. It is known from the theory of plasticity that the magnitude of the hydrostatic stress determines the extent of plastic deformation prior to fracture.[24] Various nominally brittle solids have been found to be capable of ductile behavior but only under the influence of high hydrostatic pressure.[25] An abundance of literature also demonstrated that silicon undergoes plastic deformation and phase transformation under hardness indenters and in other situations where high hydrostatic pressure exists.[9,26–33] Immediately below the indenter, the material forms a radially expanding core, exerting a uniform hydrostatic pressure on its surroundings.[34] This hydrostatic pressure ($\sim$16 GPa) can be sufficiently high to make silicon undergo a phase transformation.[29] In ultraprecision machining, the stress state in the cutting region depends on the tool–workpiece contact geometry. Since a commercially available diamond tool usually has an edge radius of a few tens of nanometers,[35–37] when the undeformed chip thickness is extremely small, the effective rake angle generated by the edge radius becomes a high negative value. This situation is geometrically akin to the indentation tests, hence it generates a similar stress state to the hydrostatic stress state produced under indenters.[7,38] Provided that the hydrostatic pressure is sufficiently high, it will cause the phase transformation of silicon.

Due to the high hydrostatic pressure (10–13 GPa), a structural transformation from diamond cubic (Si-I) into a metallic state β-Sn (Si-II) occurs.[39] However, the metallic phase is not stable at low pressure ($\sim$4 GPa). After the indenter is unloaded, the pressure-induced metallic phase does not transform back to the diamond cubic structure, but instead, changes to an amorphous phase or other metastable phases.[29,32] Similarly, in ultraprecision machining, it can be thought that first a transformation from diamond cubic structure to metallic phase occurs in front of the tool, and subsequently, a transformation from the metallic phase to amorphous phase takes place after the tool passes. Thus, the final subsurface damage layer contains an amorphous phase rather than the metallic phases. It is also worth noting that other metastable phases of silicon (Si-III, Si-XII, and Si-IV) that appeared in the low-speed scratching tests[15] were not observed in the present study. This finding is attributed to the plain strain orthogonal cutting conditions provided by the tool geometry, and the significantly higher machining speed used in this article.

The phase transformation of silicon during machining has double-faced effects. On the one hand, due to the transformation from diamond cubic to metallic structure, the material around the tool becomes sufficiently ductile to sustain plastic flow. This facilitates the ductile regime machining. On the other hand, the transformation from metallic to amorphous gives rise to the residual amorphous layer on the produced surface, which affects the optical and electronic properties of the final products.

In order to enhance the phase transformation ahead of the tool to achieve a ductile regime, it is beneficial to use tools with high negative rake angles and a large edge radius. However, a very high negative rake angle or a very large

edge radius results in an excessively large hydrostatic stress field below the tool and causes a significant downward flow of work material beneath the tool. This, in turn, leads to a thick subsurface damage layer.[18] The depth of the deformation layer and the downward flow of the work material become increasingly significant as the undeformed chip thickness increases, like that in metal cutting.[40] This might be the reason why the ductile–brittle transition boundary corresponds to the maximum intensity of the amorphous phase in the present experiments. That is, the ductile–brittle transition boundary corresponds to the highest material removal rate within the ductile regime, and causes the largest subsurface amorphization. However, as undeformed chip thickness increases beyond the critical undeformed chip thickness (d_c), the upper part of the cutting region transitions to a low-stress state,[38] and thus brittle fractures occur intermittently. The propagation of brittle fractures relieves the hydrostatic pressure ahead of the tool and phase transformation does not occur. This agrees well with the measurement results on residual stress of machined silicon and germanium surfaces. That is, in damaged areas the stresses were tensile, while in undamaged areas the stresses were compressive.[20] This leads to the location dependence of Raman spectra in the brittle regime. However, this location dependence could not be identified by means of laser macro-Raman tests due to the averaging effects.[21]

The results from the present study demonstrate two possibilities. One is the possibility of evaluating the degree of the subsurface amorphization, namely, the depth of the subsurface amorphous layer, by using laser micro-Raman intensity, which has not been taken into account in previous studies. The other possibility is to eliminate subsurface amorphization by optimizing the machining conditions and tool geometries. A conclusion from this study is that, in order to thin the subsurface amorphous layer, it is essential to use as small an undeformed chip thickness as possible ($\sim$50 nm). Another empirical supposition is that a tool with a moderate negative rake angle and a sharp cutting edge will be beneficial for reducing subsurface damage compared to a tool with a high negative rake angle and a blunt cutting edge.

V. CONCLUSIONS

(1) Under high-speed and plain strain conditions, the subsurface layer of a machined silicon substrate was partially transformed to the amorphous phase, the Raman intensity of an amorphous phase depending on the undeformed chip thickness. Other metastable phases which appeared in low-speed scratching tests were not observed in the present experiments.
(2) The Raman intensities of the crystalline phase and the amorphous phase show reverse tendencies with respect to the undeformed chip thickness.
(3) In the brittle machining regime, the Raman characteristics of the surface depend on the locations of test points. The nonfractured areas show the presence of the amorphous phase, while the fractured areas remain crystalline.
(4) The critical undeformed chip thickness for the ductile–brittle transition was 150 nm. Near the ductile–brittle transition boundary, the intensity of the crystalline phase reaches a minimum while the intensity of the amorphous phase reaches a maximum value.
(5) In the ductile machining regime, the intensity of the amorphous phase decreases sharply as the undeformed chip thickness decreases below 50 nm.
(6) The hydrostatic pressure condition generated by the high negative effective rake angle is the origin of the phase transformation. It is possible to eliminate the subsurface amorphization damage by optimizing the tool geometries and the machining conditions.

ACKNOWLEDGMENTS

The author is grateful to Dr. H. Kimiwada and Dr. Y. Ohkubo of the JASCO Corporation for assistance with laser micro-Raman tests. Thanks are extended to Dr. J. A. Patten of the Center for Precision Metrology, the University of North Carolina at Charlotte, and Dr. Y. Abe of the Department of Material Science, Kitami Institute of Technology, for their discussion. This work has been financially supported by a Grant-in-Aid for Young Scientists from the Ministry of Education, Science, Sports, and Culture of Japan.

[1] J. Yan, K. Syoji, and T. Kuriyagawa, J. Jpn. Soc. Precis. Eng. **68**, 1561 (2002).
[2] S. G. Kaplan and L. M. Hanssen, Infrared Phys. Technol. **43**, 389 (2002).
[3] T. Nakasuji, S. Kodera, S. Hara, H. Matsunaga, N. Ikawa, and S. Shimada, Ann. CIRP **39**, 89 (1990).
[4] P. N. Blake and R. O. Scattergood, J. Am. Ceram. Soc. **73**, 949 (1990).
[5] T. Shibata, S. Fujii, E. Makino, and M. Ikeda, Precis. Eng. **18**, 130 (1996).
[6] J. Yan, K. Syoji, and T. Kuriyagawa, J. Jpn. Soc. Precis. Eng. **65**, 1008 (1999).
[7] J. Yan, M. Yoshino, T. Kuriyagawa, T. Shirakashi, K. Syoji, and R. Komanduri, Mater. Sci. Eng., A **297**, 230 (2001).
[8] K. E. Puttick, L. C. Whitmore, C. L. Chao, and A. E. Gee, Philos. Mag. A **69**, 91 (1994).
[9] J. C. Morris and D. L. Callahan, J. Mater. Res. **9**, 2907 (1994).
[10] J. C. Morris, D. L. Callahan, J. Kulik, J. A. Patten, and R. O. Scattergood, J. Am. Ceram. Soc. **78**, 2015 (1995).
[11] B. V. Tanikella, A. H. Somasekhar, A. T. Sowers, R. J. Nemanich, and R. O. Scattergood, Appl. Phys. Lett. **69**, 2870 (1996).
[12] T. Shibata, A. Ono, K. Kurihara, E. Makino, and M. Ikeda, Appl. Phys. Lett. **65**, 2553 (1994).
[13] C. Jeynes, K. E. Puttick, L. C. Whitmore, K. Gartner, A. E. Gee, D. K. Millen, R. P. Webb, R. M. A. Peel, and B. J. Sealy, Nucl. Instrum. Methods Phys. Res. B **118**, 431 (1996).
[14] Y. Gogotsi, C. Baek, and F. Kirscht, Semicond. Sci. Technol. **14**, 936 (1999).
[15] Y. Gogotsi, G. Zhou, S. Ku, and S. Cetinkunt, Semicond. Sci. Technol. **16**, 345 (2001).
[16] U. Bismayer, E. Brinksmeier, B. Güttler, H. Seibt, and C. Menz, Precis. Eng. **16**, 139 (1994).
[17] J. Yan, K. Syoji, T. Kuriyagawa, and H. Suzuki, J. Mater. Process. Technol. **121**, 363 (2002).
[18] J. Yan, K. Syoji, and T. Kuriyagawa, J. Japan Soc. Prec. Eng. **66**, 1130 (2000).
[19] J. Yan, K. Syoji, and J. Tamaki, Wear **255**, 1380 (2003).
[20] R. G. Sparks and M. A. Paesler, Precis. Eng. **10**, 191 (1988).
[21] P. S. Pizani, R. Jasinevicius, J. G. Duduch, and A. J. V. Porto, J. Mater. Sci. Lett. **18**, 1185 (1999).
[22] H. Richter, Z. P. Wang, and L. Ley, Solid State Commun. **39**, 625 (1981).
[23] A. Zwick and R. Carles, Phys. Rev. B **48**, 6024 (1993).
[24] W. Johnson and P. B. Mellor, *Engineering Plasticity* (Van Nostrand Reinhold, London, 1973).
[25] P. W. Bridgman, J. Appl. Phys. **18**, 246 (1947).

[26] I. V. Gridneva, Y. V. Milman, and V. I. Trefilov, Phys. Status Solidi A **14**, 177 (1972).
[27] V. G. Eremenko and V. I. Nikitenko, Phys. Status Solidi A **14**, 317 (1972).
[28] M. J. Hill and D. J. Rowcliffe, J. Mater. Sci. **9**, 1569 (1974).
[29] D. R. Clarke, M. C. Kroll, P. D. Kirchner, and R. F. Cook, Phys. Rev. Lett. **60**, 2156 (1988).
[30] G. M. Pharr, W. C. Oliver, and D. S. Harding, J. Mater. Res. **6**, 1129 (1991).
[31] D. L. Callahan and J. C. Morris, J. Mater. Res. **7**, 1614 (1992).
[32] A. Kailer, Y. G. Gogotsi, and K. G. Nickel, J. Appl. Phys. **81**, 3057 (1997).
[33] J. E. Bradby, J. S. Williams, J. Wong-Leung, M. V. Swain, and P. Munroe, Appl. Phys. Lett. **77**, 3749 (2000).
[34] K. L. Johnson, J. Mech. Phys. Solids **18**, 115 (1970).
[35] S. Asai, Y. Taguchi, K. Horio, T. Kasai, and A. Kobayashi, Ann. CIRP **39**, 85 (1990).
[36] I. Miyamoto, T. Ezawa, and K. Nishimura, Nanotechnology **1**, 44 (1990).
[37] R. Komanduri, N. Chandrasekaran, and L. M. Raff, Wear **219**, 84 (1998).
[38] J. Yan, K. Syoji, and T. Kuriyagawa, *Proceedings of the International Conference on Advanced Manufacturing Systems and Manufacturing Automation*, Guangzhou, China, 19–21 June 2000 (Guangdong People's Publishing House, Beijing, 2000), pp. 185–189.
[39] R. J. Needs and A. Mujica, Phys. Rev. B **51**, 9652 (1995).
[40] R. Komanduri, Int. J. Mach. Tool Des. Res. **11**, 223 (1971).